THE JOURNAL OF PHYSICAL CHEMISTRY B

Article

pubs.acs.org/JPCB

Role of *in Situ* Resultant H_2O_2 in the Visible-Light-Driven Photocatalytic Inactivation of *E. coli* Using Natural Sphalerite: A Genetic Study

Huixian Shi,[†,§] Guocheng Huang,[†] Dehua Xia,[†] Tsz Wai Ng,[†] Ho Yin Yip,[†] Guiying Li,[§] Taicheng An,*[,§] Huijun Zhao,[‡] and PoKeung Wong*[,†]

[†]School of Life Sciences, The Chinese University of Hong Kong, Shatin, NT, Hong Kong SAR, China

[§]State Key Laboratory of Organic Geochemistry and Guangdong Key Laboratory of Environmental Protection and Resources Utilization, Guangzhou Institute of Geochemistry, Chinese Academy of Sciences, Guangzhou 510640, China

[‡]Centre for Clean Environment and Energy, Griffith School of Environment, Griffith University, Nathan, Queensland 4222, Australia

Supporting Information

ABSTRACT: This study investigated how a natural sphalerite (NS) photocatalyst, under visible light irradiation, supports photocatalytic bacterial inactivation. This was done by comparing parent *E. coli* BW25113, and its two isogenic single-gene knock-out mutants, *E. coli* JW0797-1 (*dps*$^-$ mutant) and JW1721-1 (*katE*$^-$ mutant), where both *dps* and *KatE* genes are likely related to H_2O_2 production. NS could inactivate approximately 5-, 7- and 7-log of *E. coli* BW25113, JW0797-1, and JW1721-1 within 6 h irradiation, respectively. The two isogenic mutants were more susceptible to photocatalysis than the parental strain because of their lack of a defense system against H_2O_2 oxidative stress. The ability of *in situ* resultant H_2O_2 to serve as a defense against photocatalytic inactivation was also confirmed using scavenging experiments and partition system experiments. Studying catalase activity further revealed that *in situ* H_2O_2 played an important role in these inactivation processes. The destruction of bacterial cells from the cell envelope to the intracellular components was also observed using field emission-scanning electron microscopy. Moreover, FT-IR was used to monitor bacterial cell decomposition, key functional group evolution, and bacterial cell structures. This is the first study to investigate the photocatalytic inactivation mechanism of *E. coli* using single-gene deletion mutants under visible light irradiation.

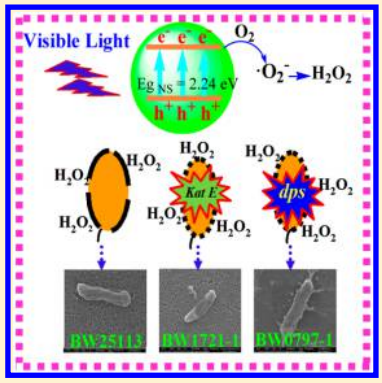

INTRODUCTION

Contaminated water is a significant source of potentially hazardous microorganisms that can cause severe human health problems.[1] Although conventional water disinfection processes such as ozonization, chlorination, adsorption, and membrane separation effectively eliminate most pathogenic microorganisms, they have various drawbacks. These drawbacks include harmful disinfection byproduct production, high costs, or low efficiencies.[2,3] Since a TiO_2−UV photocatalytic system was first used to successfully inactivate three different microorganisms in 1985,[4] photocatalytic technology has been extensively tested and has been proven to be a cost-effective, safe, and environmentally friendly alternative for water disinfection.[5,6] However, most studies mainly focus on disinfection performance under UV light irradiation; the inactivation mechanism of the bacteria has seldom been investigated. Recently, the role of the fatty acid profile and coenzyme A in photocatalytic bacteria inactivation were systemically investigated using TiO_2 under UV light irradiation.[7] Nevertheless, using UV light significantly constrains photocatalytic technology use because of its low solar energy efficiency and quantum efficiency. As such, recent effort has been devoted to develop high cost-effective visible-light-driven (VLD) photocatalysts. However, although they showed promising disinfection performance under visible light (VL), most VLD photocatalysts were synthetic and produced in small amounts.[8−12] Today, the massive production of such synthetic photocatalysts is very expensive, which has limited large scale use. Compared with synthetic photocatalysts, naturally occurring materials cost less and are readily accessible. Previously, a new kind of natural sphalerite (NS) was successfully used to inactivate bacteria; the e^- and H_2O_2 were found to be the major reactive oxygen species (ROSs) in this process.[13,14] That is, in the NS-VL system, the resultant H_2O_2 plays an important indirect role in the photocatalytic inactivation process.[14] Thus, the role of *in situ* H_2O_2 needs further validation at the gene level. Unfortunately, the genetic function and the role of bacterial cellular components in the bacterial photocatalytic inactivation process are not well understood at this time.

The typical physiological role of catalase (CAT) within bacteria is to remove H_2O_2, an ROS, before it causes cellular damage.[15] Although most bacteria encode multiple catalases,

Received: November 8, 2014
Revised: January 15, 2015
Published: January 20, 2015

DOI: 10.1021/jp511201w
J. Phys. Chem. B 2015, 119, 3104−3111

two different CATs, a bifunctional catalase HPI and a monofunctional catalase HPII,[16] were used to investigate the role in *E. coli* in this study. The *katE* encoding HPII, an important kind of catalase, has been extensively characterized physically, kinetically, and structurally.[17] The *dps*, a kind of DNA binding protein from starved *E. coli* cells, is a member of ferritin superfamily. It prevents DNA oxidative damage during the photocatalytic process.[18] In addition, a few studies have reported that ROSs, such as *in situ* H_2O_2, can cause cell membrane and DNA damage during the photocatalytic processes.[19] However, in the NS-VL system, we do not know whether these ROSs (like *in situ* resultant H_2O_2), can cause *E. coli* inactivation, and whether bacterial inactivation contributes to DNA damage in cellular components. Also, the influence of CAT on the photocatalytic inactivation mechanism is not fully elucidated at the gene level.

This study explored the photocatalytic inactivation mechanism of *E. coli*, using *E. coli* BW25113 (parental strain) and its two isogenic single-gene knock-out mutants *E. coli* JW0797-1 (*dps*$^-$ mutant) and *E. coli* JW1721-1 (*katE*$^-$ mutant). First, the photocatalytic inactivation efficiencies of the parent and two mutants were compared in the NS-VL system. Second, we attempted to define the relationship between CAT activity and the photocatalytic inactivation efficiency of these bacterial strains. Finally, the mechanism for the involvement of different ROSs, especially *in situ* resultant H_2O_2, were also proposed in the photocatalytic inactivation of *E. coli* in the NS-VL system under visible light irradiation.

EXPERIMENTAL SECTION

Photocatalyst. The NS used in this study was collected from a mining site.[13,14] After being mechanically crushed and milled at the mine sites, the NS particles were passed through different sieves. The resultant powder with a particle size of less than 40 μm was used directly.

Bacterial Strains. The parent *E. coli* BW25113, and the single-gene deletion *dps*$^-$ mutant (*E. coli* JW0797-1 carrying the mutation of *dps*784(del::kan)) and *katE*$^-$ mutant (*E. coli* JW1721-1 carrying the mutation of *katE*731(del::kan)) derivatives of *E. coli* K-12 (Table 1) were chosen as the model bacteria and purchased from the Coli Genetic Stock Center (CGSC, Yale University, New Haven, CT, USA). The bacterial cells were cultured in nutrient broth (BioLife, Milano, Italy) solution at 37 °C for 16 h with shaking and then washed with sterilized saline for later use.

Table 1. Genetic Information of Parental Strain (*E. coli* BW25113) and Its Single-Gene Knock out Mutants (*E. coli* JW0797-1 and *E. coli* JW1721-1)

strain name	deleted gene	CGSC mutation name	mutation function
E. coli BW25113	None		not appropriable
E. coli JW0797-1	*dps*	*dps*784(del)::kan	DNA-binding protein, starvation-induced resistant to H_2O_2
E. coli JW1721-1	*katE*	*katE*731(del)::kan	catalase

Photocatalytic Inactivation Process. The experimental procedure of the photocatalytic inactivation was described in our previous study,[14] and a fluorescent tube (FlT) was selected as VL source with intensity of 100 mW·m^{-2}. In brief, inactivation was carried out in a photocatalytic reactor (Figure S1, Supporting Information). The photocatalyst (1 g·L^{-1}) and the washed bacterial cell suspension were then added into the reactor, and the cell density was adjusted to 1.5×10^7 colony forming units per milliliter (cfu·mL^{-1}). All reaction suspensions were stirred in the dark for 120 min to establish an adsorption−desorption equilibrium before the reaction. After the photocatalytic inactivation, an aliquot of the reaction solution was sampled and immediately diluted it with sterilized saline solution (0.9% NaCl). The appropriate diluted sample was spread on nutrient agar and incubated at 37 °C for 18 h, then the number of colonies formed was counted to determine the number of viable cells to analyze the bacterial concentration. To further probe whether direct contact between photocatalyst and bacterial cell occurred, a partition system (Figure S2, Supporting Information) was used to separate bacteria from the photocatalyst surface.[14,20,21] All the experiments were conducted in triplicates.

Analysis. *Fluorescence Spectroscopy.* Following the recommended procedure in the bacterial viability kit, aliquot samples of bacteria before and after the photocatalytic treatment were collected and stained with typical cell-labeling dye mixtures of SYTO 9 (a green-fluorescent nucleic acid dye) and propidium iodide (PI, a red-fluorescent nucleic acid dye) to detect living and dead bacterial cells, respectively. After incubation at 25 °C in the dark for 15 min, the samples were transferred to the coverslip and observed with a fluorescence microscope (Nikon ECLIPSE 80i, Japan) equipped with a filter block NUV-2A consisting of excitation filter Ex 400-680 (Nikon, Japan) and Spot-K slider CCD camera (Diagnostic Instruments Inc., USA).[22] A FlT was selected as VL source with intensity of 100 mW·m^{-2}.

Field Emission Scanning-Electron Microscopy (FESEM). The reaction suspensions before and after the photocatalytic treatment were collected and centrifuged. Then, the bacterial cell was prefixed with glutaraldehyde (2.5%) for 4 h. After that, the bacterial cells were mounted on a glass slide (treated with 0.1% polylysine) and then washed with PBS (phosphate buffer 0.1%) for 20 min five times. Subsequently, bacterial cells were sequentially dehydrated, with a gradual series of ethanol (30% for 15 min, 50% for 15 min, 70 for 12 h, 90% for 15 min, and then 100% for 15 min 3 times), and then with 100% butyl alcohol for 15 min three times. The treated bacterial cells were finally critical point freeze-dried; gold sputter was coated on the substrates; and cells were visualized using a FESEM (JEOL JSM-6330F, Japan).

Fourier Transform-Infrared (FT-IR) Spectroscopy. The experimental suspensions were collected at different times, and evaporated by a freeze-drying method. The dry residue was then supported onto KBr pellets for measurement using a FT-IR spectrometer (FTS-4000 Varian Excalibur, USA).

Leakage of Potassium Ion (K^+). To investigate K^+ leakage from bacterial cells during photocatalytic inactivation, samples were collected and filtered before and after different treatments through a Millipore filter with pore size of 0.22 μm. After filtration, the K^+ concentration was measured using a polarized Zeeman atomic absorption spectrophotometer (AAS) (Hitachi Z-2300, Japan).

CAT Activity. The CAT activity assay was conducted using the CAT Assay Kit (Cayman Chemical Co., Ann Arbor, MI, USA), following the manufacturer's recommended protocol. One unit of CAT activity (nmol·min^{-1}·mL^{-1}) was defined as

DOI: 10.1021/jp511201w
J. Phys. Chem. B 2015, 119, 3104−3111

the amount of enzyme that causes the formation of 1 nmol formaldehyde min^{-1} at 25 °C.

Statistical Analysis. Statistical significance determined using the Student two-tail *t* test. The anova was used for multiple comparisons. Differences between groups were considered significant if $p \leq 0.05$.

RESULTS AND DISCUSSION

Photocatalytic Inactivation Performance. Figure 1 illustrates the photocatalytic inactivation efficiencies of the parental strain (*E. coli* BW 25113) and its single-gene knock-out mutants *dps*$^-$ (*E. coli* JW0797-1) and *katE*$^-$ (*E. coli* JW1721-1) by NS under visible light irradiation. The dark and light controls (Figure S3, Supporting Information) showed no obviously change in the bacterial population, indicating that the light or NS caused no toxic effect to the bacteria on their own. When NS was irradiated by VL, approximately 5-log inactivation of *E. coli* BW25113 could be achieved after 6 h photocatalytic treatment. Nevertheless, both mutants (about 7-log) could be completely inactivated within 6 h, indicating that the two mutants exhibited higher susceptibilities toward the photocatalytic inactivation as compared to the parental strain (2.24 ± 0.46-log for the parental strain vs 0-log for the two mutants at 6 h photocatalytic treatment, $p \leq 0.05$).

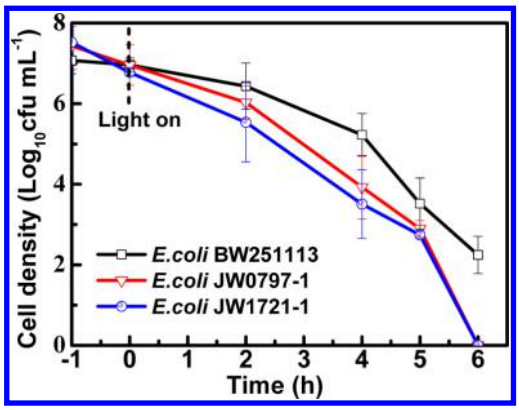

Figure 1. Comparison of photocatalytic inactivation efficiencies of *E. coli* BW25113, *E. coli* JW0797-1 and *E. coli* JW1721-1 in the NS-FlT system. Data expressed as mean ± standard deviation (SD); bars, SD; $n = 3$.

In addition, the Hom model was employed to evaluate the photocatalytic inactivation kinetics of the bacteria.[23−25] Photocatalytic inactivation begins with an initial smooth decay, known as the "shoulder", followed by a fast inactivation region, and ending with a long deceleration process after disinfection, known as "tail".[25] This model can be matched using the Microsoft Excel tool GInaFIT.[26] Using this tool, three parameters from the three steps above can be obtained. These calculated parameters describe the kinetics of photocatalytic inactivation process, as shown in Table S1 (Supporting Information). Notably, for the parent (*E. coli* BW 25113), the highest inhibition time (S_L) and the lowest inactivation rate (k_{max} in the second step), compared with those of its single-gene knock-out mutant *dps*$^-$ (*E. coli* JW0797-1) and *katE*$^-$ (*E. coli* JW1721-1), were seen under visible light irradiation. This suggests that the cell density of *dps*$^-$ and *katE*$^-$ mutants decreased slightly faster than with the parental strain. This conclusion is consistent with the photocatalytic inactivation results shown in Figure 1; possible reasons will be discussed below.

The photocatalytic activation performance of the parent and mutants in the NS-FlT system was further confirmed using the BacLight kit fluorescent microscopic method (Figure 2). The viable cells appear as green, and the dead cells with damaged cell membranes are red.[27] In this NS-FlT system, it took less time to completely inactivate the same concentration of *dps*$^-$ and *katE*$^-$ mutants than with the parental strain. This is consistent with the result of photocatalytic inactivation kinetics shown in Figure 1.

Photocatalytic Inactivation Mechanism of *E. coli*. Specifying Reactive Species (RSs). Generally, various RSs, such as H_2O_2, $^{\bullet}O_2^-$, $^{\bullet}OH$, h^+, and e^-, are produced *in situ* during the photocatalytic process. To determine which RSs play an important role in the VLD photocatalytic inactivation of bacteria in this system, different individual scavengers were used to remove the respective RSs. Scavengers used in this study included $Na_2C_2O_4$ for h^+, Cr(VI) for e^-, EDTA-Fe(II) for H_2O_2, 2-propanol for $^{\bullet}OH$, and 4-hydroxy-2,2,6,6-tetramethylpiperidinyloxy (TEMPOL) for $^{\bullet}O_2^-$.[28−30] As Figure 3 shows, without adding any scavenger, approximately 5-, 7-, and 7-log inactivation were achieved for *E. coli* BW25113, JW0797-1, and JW1721-1, respectively, within 6 h VL irradiation. With 2-propanol removing $^{\bullet}OH$, the bacterial density decreased 3.9-, 4.9-, and 4.6-log for *E. coli* BW25113, JW0797-1, and JW1721-1, respectively. That is, $^{\bullet}OH$ contributed to 3.1-, 2.1-, and 2.4-log inactivation efficiencies, suggesting that $^{\bullet}OH$ plays a moderate role in the photocatalytic inactivation process. However, the obvious inhibition effect was observed for the three strains when $Na_2C_2O_4$ (h^+ scavenger) was used; the bacterial density decreased by 2.4-, 3.0-, and 2.7-log for *E. coli* BW25113, JW0797-1, and JW1721-1, respectively. This means h^+ contributed to 4.6-, 4.0-, and 4.3-log inactivation; h^+ was confirmed to be important in this phototcatalytic inactivation process.

When the Cr (VI) (e^- scavenger) was added, the bacterial cell density decreased 3.3-, 4.6-, and 3.6-log for *E. coli* BW25113, JW0797-1, and JW1721-1, respectively. This demonstrates e^- contributed to 3.7-, 2.4-, and 3.4-log reduction of the bacterial cell density, playing a moderate role in this process. With the addition of TEMPOL, the photocatalytic inactivation efficiency remained the same as not adding a scavenger, indicating that $^{\bullet}O_2^-$ is not directly involved in the photocatalytic inactivation system. In the presence of Fe (II) to remove H_2O_2, the bacterial cell density decreased 2.5-, 3.9-, and 3.2-log for *E. coli* BW25113, JW0797-1, and JW1721-1, respectively. This indicated that *in situ* H_2O_2 is the dominant species involved in the photocatalytic inactivation in the NS-FlT system. Under VL irradiation, we hypothesize that the photocatalyst is first activated to generate e^- at the NS conduction band. The conduction band e^- can react with soluble O_2 to produce reactive $^{\bullet}O_2^-$, and react with H_2O to form $^{\bullet}OOH$, and then further form *in situ* H_2O_2. To further understand the roles of H_2O_2 and h^+, argon (Ar) was aerated in the system to remove O_2. As the reactive oxidative species were inhibited, the production of H_2O_2 decreased. As Figure 4 shows, under anaerobic condition, when the Cr (VI) and $Na_2C_2O_4$ were added to remove e^- and h^+, the photocatalytic inactivation efficiency was completely inhibited. This confirms that *in situ* H_2O_2 and h^+ act as the main RSs in this photocatalytic activation process.

DOI: 10.1021/jp511201w
J. Phys. Chem. B 2015, 119, 3104−3111

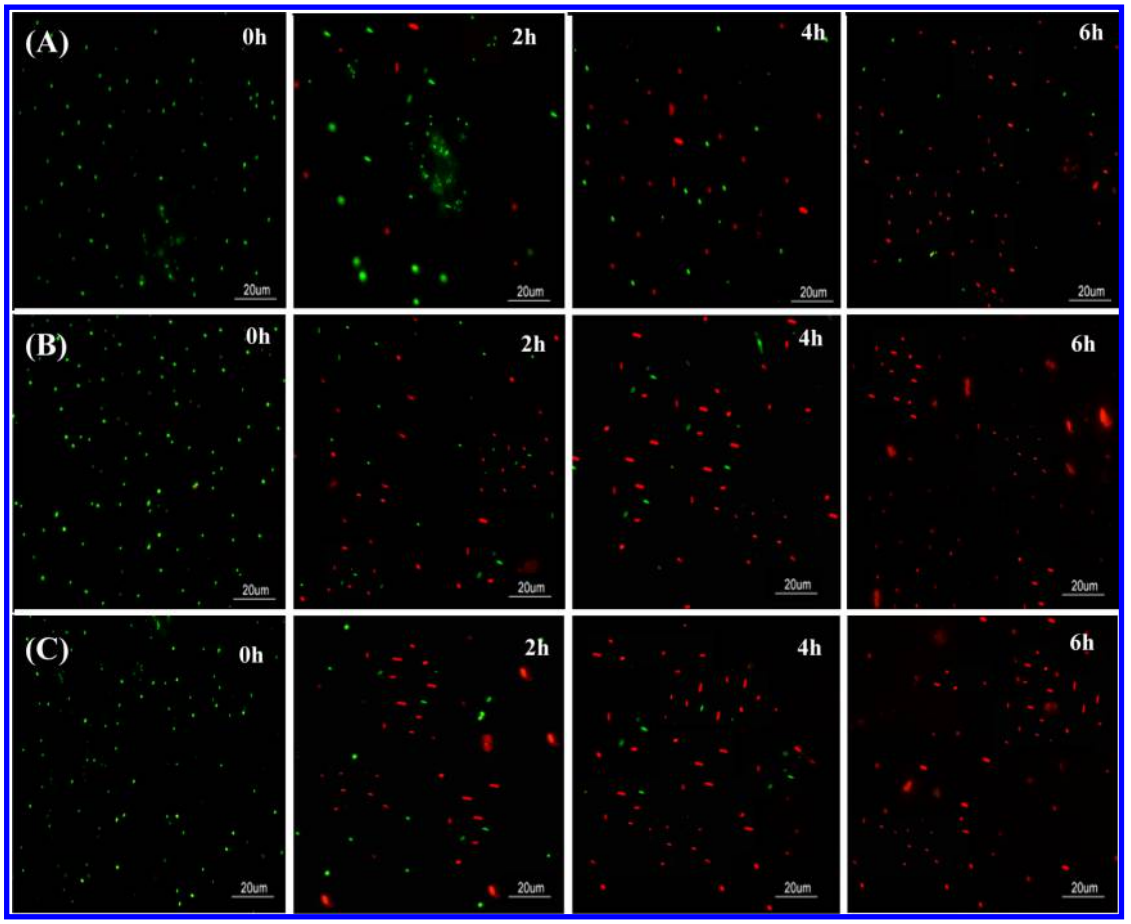

Figure 2. Fluorescence microscopic images of bacterial cells after different treatment intervals in the NS-FlT system: (A) *E. coli* BW25113, (B) *E. coli* JW0797-1, and (C) *E. coli* JW1721-1.

Role of in Situ Resultant H_2O_2. The dps^- and $katE^-$ mutants are both related to the H_2O_2 metabolism, so partition system experiments (Figure S2, Supporting Information) were conducted to further confirm the role of *in situ* H_2O_2 in this photocatalytic inactivation process.[27,28] For this experiment, the bacterial suspension was injected into a semipermeable membrane tube, while NS was dispersed outside of the membrane tube. NS particles with a diameter of approximately 1−40 μm, and the bacterial weight of about 2.6×10^6 Da, cannot pass through the semipermeable membrane. As such, the bacterial cells and NS particles cannot directly come into contact, but small molecules such as water and *in situ* H_2O_2 molecules can freely pass through the membrane tube during the photocatalytic inactivation. As Figure S4 (Supporting Information) shows, in the partition system, approximately 4.0-, 7.0-, and 7.0-log of *E. coli* BW25113, JW0797-1, and JW1721-1 were inactivated within 6 h, respectively.

Although the inactivation efficiencies are the same for the two mutants in the two systems (partitioned and non-partitioned), the inactivation efficiency for *E. coli* BW25113 is slightly lower in the partition system than in the nonpartition system (5-log reduction). This indicated that direct contact of NS particles with bacteria cells is not fully required in this photocatalytic inactivation system. This further indicates that some long lifetime RSs, such as H_2O_2, play an important role in killing bacteria in this system; the *in situ* H_2O_2 outside the semipermeable membrane diffuses into the partition system and serves as the bactericide. Furthermore, in both nonpartition (Figure 1) and partition systems (Figure S4, Supporting Information), the photocatalytic inactivation efficiencies of two mutants are much higher than the parental strain (*E. coli* BW25113). This further confirms that H_2O_2 played a critical role in this system, because both mutants experience a shortage of defense activity against H_2O_2 oxidative stress.

To further validate the role of *in situ* resultant H_2O_2 in this system, H_2O_2 was also directly added into the system. As Figure S5 (Supporting Information) shows, when 5 mM H_2O_2 was added into the system, approximately 7.0-log cells of three bacterial strains were completely inactivated within 3 h. Further, two mutants showed higher susceptibility toward photocatalytic inactivation and decreased faster than the parental strain. Moreover, the photocatalytic inactivation efficiency in the H_2O_2-NS-FlT system (Figure S5, Supporting Information) is higher than that in the system without H_2O_2 (Figure 1), indicating the critical role H_2O_2 plays in the photocatalytic inactivation process.

From the photocatalytic inactivation kinetic results (Table S1, Supporting Information), the inhibition time (S_L, 2.37 min) of *E. coli* JW1721-1 is shorter than that of parental strain *E. coli* BW25113 (2.94 min), because *E. coli* JW1721-1 is a catalase gene defect mutant. Thus, CAT production is much lower for this mutant than for the parental strain, so *E. coli* JW1721-1 is more easily attacked by *in situ* resultant H_2O_2 during the initial stage of photocatalytic inactivation. Similarly, the inhibition time of *E. coli* JW0797-1 (2.62 min) is also slightly shorter than that of parental strain *E. coli* BW25113 (2.94 min). This is

DOI: 10.1021/jp511201w
J. Phys. Chem. B 2015, 119, 3104−3111

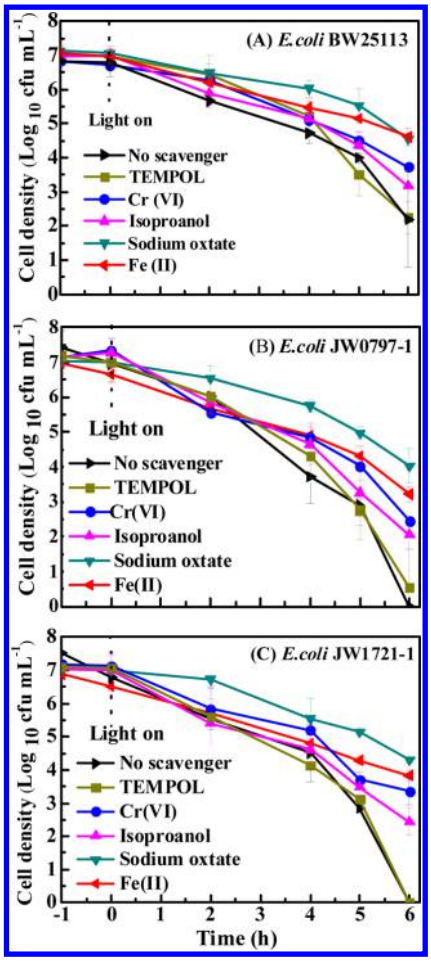

Figure 3. Inactivation efficiencies of bacteria in the NS-VL system with different scavengers (0.5 mM 2-propanol, 0.5 mM $Na_2C_2O_4$, 50 μM Cr(VI), 2 mM TEMPLO, and 0.1 mM Fe(II)−EDTA). Data expressed as mean ± standard deviation (SD); bars, SD; n = 3.

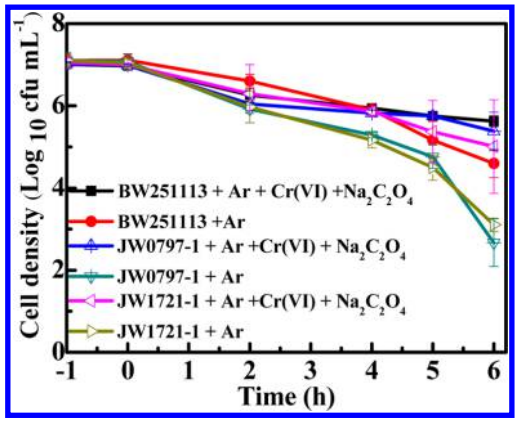

Figure 4. Photocatalytic inactivation efficiencies under anaerobic condition with the addition of scavengers. Data expressed as mean ± standard deviation (SD); bars, SD; n = 3.

explained by the deletion of the *dps* gene in *E. coli* JW0797-1, reducing resistance to H_2O_2 attack, and making it easier to be attacked by *in situ* H_2O_2 during the initial stage of the photocatalytic inactivation compared with the parental strain. In addition, the inactivation rates (k_{max}) of JW1721-1 and *E. coli* JW0797-1 are 5.21 and 4.18 cfu·mL^{-1} min^{-1}, respectively, which are larger than that of parental strain *E. coli* BW25113 (3.41 cfu·mL^{-1} min^{-1}). The results also confirm that the two mutants are more easily inactivated than the parent, because higher k_{max} indicates higher inactivation efficiency.

CAT, a kind of antioxidant enzyme in the bacterial cell, can decompose H_2O_2 to H_2O and O_2. Thus, a significantly high CAT activity within the bacteria indicates that the bacterial cells encountered a H_2O_2 attack (CAT activity for the parental strain vs the two mutants after 2 h photocatalytic treatment, $p \leq 0.05$). Therefore, CAT activity trends for three bacterial strains were analyzed during the photocatalytic inactivation process (Figure 5). CAT activity trends across the three strains were

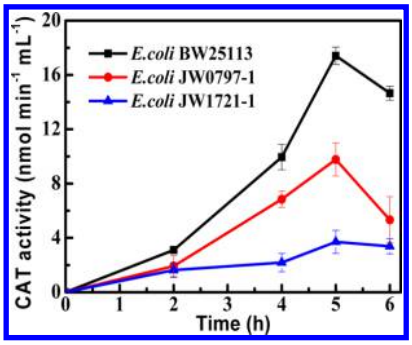

Figure 5. CAT activity in the photocatalytic inactivation of bacterial in the NS-VL system. Data expressed as mean ± standard deviation (SD); bars, SD; n = 3.

very similar, except for CAT levels. That is, CAT activity increased slowly during the initial 4 h, then increased swiftly, peaked at 5 h, and then decreased with prolonged reaction time. This indicated that a large amount of *in situ* H_2O_2 was gradually produced, attacking bacterial cells at the initial stage, and subsequently gradually activating CAT to defend from the oxidation stress from H_2O_2. The low photocatalytic inactivation efficiency at the initial stage (Figure 1) is due to protection of CAT in the bacterial cell from the RSs damage. As reaction time lengthens, the decrease of CAT activity and the rapid increase of the photocatalytic inactivation efficiency suggests that the H_2O_2 generated in the system quickly exceeds the CAT protection capability in the bacterial cell.

This result supports the previous conclusion that *in situ* resultant H_2O_2 plays an important role in the photocatalytic inactivation in the NS-FlT system. As mentioned, the CAT activity trends across the three strains were very similar, but the CAT activity of *E. coli* BW25113 is higher than both mutants, particularly *E. coli* JW1721-1. This is because *E. coli* JW1721-1 is a catalase gene defect mutant; thus, CAT production amount is lower than the parental strain, leading to much higher photocatalytic inactivation of *E. coli* JW1721-1. As for *E. coli* JW0797-1, the CAT activity is lower than the parental strain during the photocatalytic process. This is because *E. coli* JW0797-1 is a *dps* gene defect mutant, making it easier to be attacked by H_2O_2. The enzyme activity was lost when the bacterial cells were attacked by H_2O_2.

To directly confirm H_2O_2 production and its role in photocatalytic inactivation, the *in situ* H_2O_2 in the NS-FlT system was further detected using a photometric method involving peroxidase.[31] Figure S6 (Supporting Information) shows H_2O_2 absorbance (at 551 nm) against the photocatalytic inactivation time in NS-FlT system. Throughout the 6 h reaction, the H_2O_2 concentrations were greater for *E. coli* JW1721-1 (*katE*$^-$ mutant) than for JW0797-1 (*dps*$^-$ mutant),

DOI: 10.1021/jp511201w
J. Phys. Chem. B 2015, 119, 3104−3111

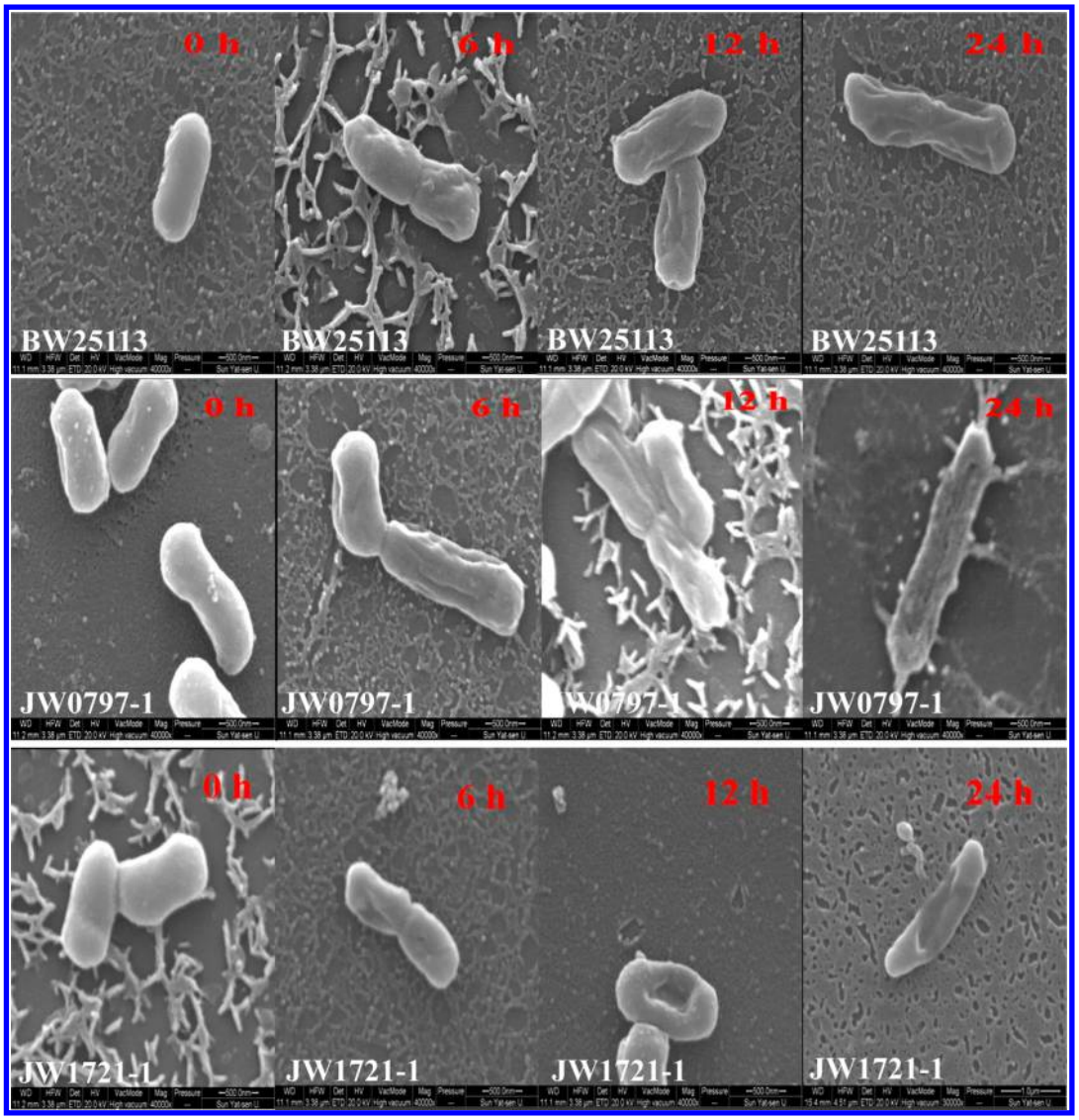

Figure 6. FE-SEM images of *E. coli* BW25113, *E. coli* JW0797-1, and *E. coli* JW1721-1 bacterial cells after different treatment intervals in the NS-FlT system.

which was greater than BW25113. This may be due to the deletion of the *katE* gene (CAT producing gene) in *E. coli* JW1721-1, leading to the loss of defenses against H_2O_2. As for *E. coli* JW0797-1 and the parental strain, the CAT gene still functions very well, producing CAT during the photocatalytic inactivation, decomposing H_2O_2, and leading to the lower H_2O_2 concentration. Because the deleted gene *dps* of *E. coli* JW0797-1 cannot prevent DNA oxidative damage during the photocatalytic process, it is easier for *in situ* H_2O_2 to attack. In fact, the *in situ* H_2O_2 concentration is much higher than the measured value, because H_2O_2 is continuously produced and dynamically consumed. The function of the *dps* gene is to resist H_2O_2 attack, whereas *katE* is coded the CAT gene of *E. coli*, protecting cells from H_2O_2 attack.[15,16,32] As shown above, H_2O_2 is a major ROS involved in the photocatalytic inactivation in this NS-FlT system; thus, the dps^- and $katE^-$ mutants are more sensitive to photocatalytic inactivation than the parent.

Bacterial Cell Decomposition. To understand the surface damage and bacterial cell destruction in the parental strain *E. coli* BW25113 and its single-gene knock-out mutants dps^- (*E. coli* JW0797-1) and $katE^-$ (*E. coli* JW1721-1) during the photocatalytic process, bacterial cell morphology at different treatment intervals were observed using FE-SEM (Figure 6). The untreated bacterial cells showed an evenly intact morphology with a well-preserved cell wall. In contrast, part of the cell wall was clearly damaged after 6 h irradiation. Increasing the irradiation time to 12 h leads to more severe cell structure damage, with severe intracellular component leakage. Finally, after 24 h irradiation, the cell wall was greatly ruptured and the intracellular components severely lost. The extent of *E. coli* JW1721-1 and *E. coli* JW0797-1 surface damage was more serious than the parental strain (*E. coli* BW25113). This indicates both knock-out mutants were more easily attacked and decomposed.

Besides directly observing cell membrane damage by FE-SEM, K^+ leakage from the cell, can also demonstrate compromised or damaged membranes.[24,33,34] As Figure S7 (Supporting Information) shows, no obvious K^+ leakage occurred from the bacteria in the dark and light control experiments. In contrast, K^+ leakage increased steadily with prolonged inactivation time, reaching a stable value after 4 h. As such, the cell structures are confirmed to be severely distorted

DOI: 10.1021/jp511201w
J. Phys. Chem. B 2015, 119, 3104−3111

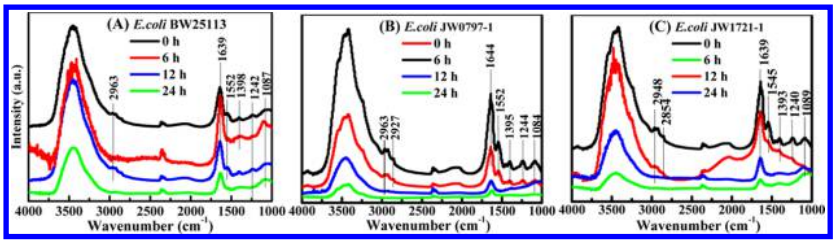

Figure 7. FT-IR spectra of (A) *E. coli* BW25113, (B) *E. coli* JW0797-1, and (C) *E. coli* JW1721-1 before and after the photocatalytic inactivation.

and the cell wall greatly ruptured. This observation indicates that the bacterial cell destruction begins with the cell wall and moves to the cellular components. Moreover, the K^+ concentration of *E. coli* JW1721-1 and *E. coli* JW0797-1 mutant is higher than the parental strain (*E. coli* BW25113), indicating that the gene knock-out mutants are more easily attacked by RSs.

To further identify the bacterial cell decomposition, the key functional groups and the bacterial cell structures were also measured using FT-IR.[35−37] Figure 7 shows FT-IR spectra of the parental strain as well as its single-gene knock-out mutants *dps*$^-$ (*E. coli* JW0797-1) and *katE*$^-$ (*E. coli* JW1721-1) as a function of time during NS photocatalytic inactivation. The biomolecular and bacteria cell functional groups were further identified, in Figure 7A−C. Characteristic peaks at approximately 2963, 2948, 2927, and 2854 cm^{-1} were assigned as ν_a (CH_3), ν_a (CH_2), ν_s (CH_3), and ν_s (CH_2), respectively. A wide band in the region 3400−3600 cm^{-1} originated from the OH group of water onto the NS surface.[35] Furthermore, there are some clear absorption peaks within the 1000−1700 cm^{-1} region, and some significant changes of the oligosaccharide bands around 1084−1089 cm^{-1} were observed. The profile changes of peaks around 1240−1244 cm^{-1} were attributed to PO_2^- vibration; the peaks around 1545−1552 and 1639−1644 cm^{-1} related to amide II and amide I, respectively. However, when the irradiation time extended to 24 h, the OH^- group absorbance intensity decayed. At this point, the peaks of C−H bands, the PO_2^- band, and amide II and amide I were nearly undetectable, indicating that the cell wall and membrane of *E. coli* BW25113, JW0797-1, and JW1721-1 were decomposed and mineralized during photocatalytic inactivation. Moreover, the intensity of the peaks of *E. coli* BW25113 were slightly stronger than those for *E. coli* JW0797-1 and *E. coli* JW1721-1 within the same 24 h. This indicates that the knock-out mutants are more easily attacked and decomposed, consistent with the photocatalytic inactivation kinetic results above.

CONCLUSIONS

This work explored the underlying photocatalytic inactivation mechanism of bacteria at the gene level, by comparing a parental bacteria strain with isogenic single-gene knock-out mutants. To date, the genetic functioning and role of bacterial cellular components in the photocatalytic inactivation of *E. coli* under visible light irradiation have not been well understood. This study, however, shows that isogenic single-gene knock-out mutants provide a new experimental method. This method allows insight into the photocatalytic inactivation mechanism, with different bacteria encoded with different genes. Furthermore, these results reveal the photocatalytic inactivation mechanism of *E. coli* in water environments, pointing to a more practical cost-efficient water disinfection technology candidate.

ASSOCIATED CONTENT

Supporting Information

Table of kinetic parameters, photograph of the setup for photocatalytic inactivation, schematic of the partition system setup, inactivation efficiencies, effect of H_2O_2 on the photocatalytic inactivation process, concentration of H_2O_2 vs the illumination time, and potassium ion leakage vs irradiation time. Supporting Information associated with this article is available free of charge via the Internet at http://pubs.acs.org.

AUTHOR INFORMATION

Corresponding Authors

*Taicheng An. Tel: +86-20-85291501. Fax: +86-20-85290706. E-mail: antc99@gig.ac.cn.

*Po Keung Wong. Tel: +852 3943 6383. Fax: +852 2603 5767. E-mail: pkwong@cuhk.edu.hk.

Notes

The authors declare no competing financial interest.

ACKNOWLEDGMENTS

This work was supported by National Natural Science Funds for Distinguished Young Scholars (41425015) and NSFC (21077104) to T. C. An and G. Y. Li, and a research grant (GRF476811) of the Research Grant Council, Hong Kong SAR Government, to P. K. Wong. Prof. Wong also expresses his thanks to the CAS/SAFEA International Partnership Program for Creative Research Teams of Chinese Academy of Sciences, China.

REFERENCES

(1) Kim, S.; Ghafoor, K.; Lee, J.; Feng, M.; Hong, J.; Lee, D. U.; Park, J. Bacterial inactivation in water, DNA strand breaking, and membrane damage induced by ultraviolet-assisted titanium dioxide photocatalysis. *Water Res.* **2013**, *47*, 4403−4411.

(2) Wang, X.; Lim, T. T. Highly efficient and stable Ag−AgBr/TiO_2 composites for destruction of *Escherichia coli* under visible light irradiation. *Water Res.* **2013**, *47*, 4148−4158.

(3) Malato, S.; Fernández-Ibáñez, P.; Maldonado, M. I.; Blanco, J.; Gernjak, W. Decontamination and disinfection of water by solar photocatalysis: Recent overview and trends. *Catal. Today* **2009**, *147*, 1−59.

(4) Matsunaga, T.; Tomoda, R.; Nakajima, T.; Wake, H. Photoelectrochemical sterilization of microbial cells by semiconductor powders. *FEMS Microbiol. Lett.* **1985**, *29*, 211−214.

(5) Zhao, H. X.; Yu, H. T.; Quan, X.; Chen, S.; Zhang, Y. B.; Zhao, H. M.; Wang, H. Fabrication of atomic single layer graphitic-C_3N_4 and its high performance of photocatalytic disinfection under visible light irradiation. *Appl. Catal., B* **2014**, *152*, 46−50.

(6) Gan, H. H.; Zhang, G. K.; Huang, H. X. Enhanced visible-light-driven photocatalytic inactivation of *Escherichia coli* by $Bi_2O_2CO_3$/Bi_3NbO_7 composites. *J. Hazard. Mater.* **2013**, *250*, 131−137.

(7) Gao, M. H.; An, T. C.; Li, G. Y.; Nie, X.; Yip, H. Y.; Zhao, H. J.; Wong, P. K. Genetic studies of the role of fatty acid and coenzyme A

DOI: 10.1021/jp511201w
J. Phys. Chem. B 2015, 119, 3104−3111

in photocatalytic inactivation of *Escherichia coli*. *Water Res.* **2012**, *46*, 3951−3957.
(8) Hu, C.; Lan, Y.; Qu, J.; Hu, X.; Wang, A. Ag/AgBr/TiO_2 Visible light photocatalyst for destruction of azodyes and bacteria. *J. Phys. Chem. B* **2006**, *110*, 4066−4072.
(9) Chang, Q.; He, H.; Zhao, J.; Yang, M.; Qu, J. Bactericidal activity of a Ce-promoted Ag/$AlPO_4$ catalyst using molecular oxygen in water. *Environ. Sci. Technol.* **2008**, *42*, 1699−1704.
(10) Ye, L.; Liu, J.; Gong, C.; Tian, L.; Peng, T.; Zan, L. Two different roles of metallic Ag on Ag/AgX/BiOX (X = Cl, Br) visible light photocatalysts: surface plasmon resonance and Z-scheme bridge. *ACS Catal.* **2012**, *2*, 1677−1683.
(11) Shi, H. X.; Chen, J. Y.; Li, G. Y.; Nie, X.; Zhao, H. J.; Wong, P. K.; An, T. C. Synthesis and characterization of novel plasmonic Ag/AgX-CNTs (X = Cl, Br, I) nanocomposite photocatalysts and synergetic degradation of organic pollutant under visible light. *ACS Appl. Mater. Interface* **2013**, *5*, 6959−6967.
(12) Shi, H. X.; Li, G. Y.; Sun, H. W.; An, T. C.; Zhao, H. J.; Wong, P.-K. Visible-light-driven photocatalytic inativation of *E. coli* by Ag/AgX-CNTs (X = Cl, Br, I) plasmonic photocatalysts: Bacterial performance and deactivation mehanism. *Appl. Catal. B: Environ.* **2014**, *158−159*, 310−307.
(13) Chen, Y. M.; Lu, A. H.; Li, Y.; Yip, H. Y.; An, T. C.; Li, G. Y.; Jin, P.; Wong, P. K. Photocatalytic inactivation of *Escherichia coli* by natural sphalerite suspension: Effect of spectrum, wavelength and intensity of visible light. *Chemosphere* **2011**, *84*, 1276−1281.
(14) Chen, Y. M.; Lu, A. H.; Li, Y.; Zhang, L. S.; Yip, H. Y.; Zhao, H. J.; An, T. C.; Wong, P. K. Naturally occurring sphalerite as a novel cost-effective photocatalyst for bacterial disinfection under visible light. *Environ. Sci. Technol.* **2011**, *45*, 5689−5695.
(15) Chelikani, P.; Fita, I.; Loewen, P. C. Diversity of structures and properties among catalases. *Cell. Mol. Life Sci.* **2004**, *61*, 192−208.
(16) Chelikani, P.; Donald, L. J.; Duckworth, H. W.; Loewen, P. C. Hydroperoxidase II of Escherichia coli exhibits enhanced resistance to proteolytic cleavage compared to other catalases. *Biochemistry* **2003**, *42*, 5729−5735.
(17) Chelikani, P.; Carpena, X.; Perez-Luque, R.; Donald, L. J.; Duckworth, H. W.; Switala, J.; Fita, I.; Loewen, P. C. Characterization of a large subunit catalase truncated by proteolytic cleavage. *Biochemistry* **2005**, *44*, 5597−5605.
(18) Kang, S.; Oltrogge, L. M.; Broomell, C. C.; Liepold, L. O.; Prevelige, P. E.; Young, M.; Douglas, T. Controlled assembly of bifunctional chimeric protein cages and composition analysis using noncovalent mass spectrometry. *J. Am. Chem. Soc.* **2008**, *130*, 16527−16529.
(19) Ashikaga, T.; Wada, M.; Kobayashi, H.; Mori, M.; Katsumura, Y.; Fukui, H.; Kato, S.; Yamaguchi, M.; Takamatsu, T. Effect of the photocatalytic activity of TiO_2 on plasmid DNA. *Mutat. Res., Genet. Tox. Environ. Mutagen.* **2000**, *466*, 1−7.
(20) Kikuchi, Y.; Sunada, K.; Iyoda, T.; Hashimoto, K.; Fujishima, A. Photocatalytic bactericidal effect of TiO_2 thin films: dynamic view of the active oxygen species responsible for the effect. *J. Photochem. Photobiol. A: Chem.* **1997**, *106*, 51−56.
(21) Wang, W. J.; Zhang, L. Z.; An, T. C.; Li, G. Y.; Yip, H. Y.; Wong, P. K. Comparative study of visible-light-driven photocatalytic mechanisms of dye decolorization and bacterial disinfection by B-Ni-codoped TiO_2 microspheres: The role of different reactive species. *Appl. Catal. B: Environ.* **2011**, *108−109*, 108−116.
(22) Shi, H. X.; Zhang, T. Y.; Li, B.; Wang, X.; He, M.; Qiu, M. Y. Photocatalytic hydroxylation of phenol with Fe−Al-silicate photocatalyst: A clean and highly selective synthesis of dihydroxybenzenes. *Catal. Commun.* **2011**, *12*, 1022−1026.
(23) Baram, Nir; Starosvetsky, David; Starosvetsy, Jeana; Epshtein, Marina Enhanced inactivation of *E. coli* bacteria using immobilized porous TiO_2 photoelectrocatalysis. *Electrochim. Acta* **2009**, *54*, 3381−3386.
(24) Baram, N.; Starosvetsky, D.; Starosvetsky, J.; Epshtein, M.; Armon, R.; Ein-Eli, Y. Photocatalytic inactivation of microorganisms using nanotubular TiO_2. *Appl. Catal. B: Environ.* **2011**, *101*, 212−219.
(25) Nie, X.; Li, G. Y.; Gao, M. H.; Sun, H. W.; Liu, X. L.; Zhao, H. J. Comparative studies on the photoelectrocatalytic inactivation of ancestor *Escherichia coli* K-12 and its mutant *Escherichia coli* BW25113 bacteria using TiO_2 nanotubes as a photoanode. *Appl. Catal. B: Environ.* **2014**, *147*, 562−570.
(26) Marugán, J.; van Grieken, R.; Sordo, C.; Cruz, C. Kinetics of the photocatalytic disinfection of *Escherichia coli* suspensions. *Appl. Catal. B: Environ.* **2008**, *82*, 27−36.
(27) Zhang, L. S.; Wong, K. H.; Yip, H. Y.; Hu, C.; Yu, J. C.; Chan, C. Y.; Wong, P. K. Effective photocatalytic disinfection of *E. coli* K-12 using AgBr-Ag-Bi_2WO_6 nanojunction system irradiated by visible light: the role of diffusing hydroxyl radicals. *Environ. Sci. Technol.* **2010**, *44*, 1392−1398.
(28) Wang, Y.; Zhang, J. Thermal stabilities of drops of burning thermoplastics under the UL 94 vertical test conditions. *J. Hazard. Mater.* **2013**, *246*, 103−109.
(29) Wang, W. J.; Yu, Y.; An, T. C.; Li, G. Y.; Yip, H. Y.; Yu, J. C.; Wong, P. K. Visible-light-driven photocatalytic inactivation of *E. coli* K-12 by bismuth vanadate nanotubes: bactericidal performance and mechanism. *Environ. Sci. Technol.* **2012**, *46*, 4599−4606.
(30) Zhang, L. S.; Wong, K. H.; Zhang, D. Q.; Hu, C.; Yu, J. C.; Chan, C. Y.; Wong, P. K. Zn:$In(OH)_yS_z$ solid solution nanoplates: synthesis, characterization, and photocatalytic mechanism. *Environ. Sci. Technol.* **2009**, *43*, 7883−7888.
(31) Bader, H.; Sturzenegger, V.; Hoigne, J. Photometric method for the determination of low concentrations of hydrogen peroxide by the peroxidase catalyzed oxidation of N,N-diethyl-*p*-phenylenediamine (DPD). *Water Res.* **1988**, *22*, 1109−1115.
(32) Alyamani, E. J.; Brandt, P.; Pena, J. A.; Major, A. M.; Fox, J. G.; Suerbaum, S.; Versalovic, J. Helicobacter hepaticus catalase shares surface-predicted epitopes with mammalian catalases. *Microbiology* **2007**, *153*, 1006−1016.
(33) Ren, J.; Wang, W. Z.; Zhang, L.; Chang, J.; Hu, S. Photocatalytic inactivation of bactrial by photocatalst Bi_2WO_6 under visible light. *Catal. Commun.* **2009**, *10*, 1940−1943.
(34) Sun, H. W.; Li, G. Y.; Nie, X.; Shi, H. X.; Wong, P. K.; Zhao, H. J.; An, T. C. Systematic approach to in-depth understanding of photoeletrocatalytic bacterial inativation mechanisms by tracking the decomposed building blocks. *Environ. Sci. Technol.* **2014**, *48*, 9412−9419.
(35) Nadtochenko, V. A.; Rincon, A. G.; Stanca, S. E.; Kiwi, J. Dynamics of *E. coli* membrance cell peroxidation during TiO_2 photocatalysis studied by ATR-FTIR spectroscopy and AFM microscopy. *J. Photochem. Photobiol. A: Chem.* **2005**, *169*, 131−137.
(36) Kiwi, J.; Nadtochenko, V. A. Evidence for the mechanism of photocatalytic degradation of the bacterila wall membrane at the TiO_2 interface by ATR-FTIR and laser kinetic spectroscopy. *Langmuir* **2005**, *21*, 4631−4641.
(37) Bacsa, R.; Kiwi, J.; Ohno, T.; Albers, P.; Nadtochenko, V. Preparation, testing and charaterization of doped TiO_2 active in the peroxidation of biomolecules under visible light. *J. Phys. Chem. B* **2005**, *109*, 5994−6003.

DOI: 10.1021/jp511201w
J. Phys. Chem. B 2015, 119, 3104−3111